Journal of Systems Engineering and Electronics
Vol. 32, No. 5, October 2021, pp.1053 – 1061

PID-type fault-tolerant prescribed performance control of fixed-wing UAV

YU Ziquan[1], ZHANG Youmin[2,*], and JIANG Bin[1]

1. College of Automation Engineering, Nanjing University of Aeronautics and Astronautics, Nanjing 211106, China;
2. Department of Mechanical, Industrial and Aerospace Engineering, Concordia University, Montreal H3G 1M8, Canada

Abstract: This paper introduces a fault-tolerant control (FTC) design for a faulty fixed-wing unmanned aerial vehicle (UAV). To constrain tracking errors against actuator faults, error constraint inequalities are first transformed to a new set of variables based on prescribed performance functions. Then, the commonly used and powerful proportional-integral-derivative (PID) control concept is employed to filter the transformed error variables. To handle the fault-induced nonlinear terms, a composite learning algorithm consisting of neural network and disturbance observer is incorporated for increasing flight safety. It is shown by Lyapunov stability analysis that the tracking errors are strictly constrained within the specified error bounds. Experimental results are presented to verify the feasibility of the developed FTC scheme.

Keywords: unmanned aerial vehicle (UAV), fault-tolerant control (FTC), prescribed performance control (PPC), proportional-integral-derivative (PID), composite learning, actuator faults.

DOI: 10.23919/JSEE.2021.000090

1. Introduction

Recently, unmanned aerial vehicles (UAVs) have been widely used to perform dangerous and tedious tasks, due to their high flexibility and large flight radius [1–4]. However, with unexpected flight scenarios, various faults encountered by a UAV may significantly degrade the maneuverability performance or even cause catastrophic accidents. To react to faults, the fault-tolerant control (FTC) concept is investigated for increasing flight safety [5–10]. In general, FTC methods can be classified into passive and active methods. With respect to the passive FTC, the robust control strategy is usually used. Regarding the active FTC, fault detection and diagnosis (FDD) is artfully incorporated into the FTC architecture to compensate for the faults [11,12]. By using such a strategy, the faulty system can be stabilized in a timely manner.

By using terminal sliding mode control (TSMC) architecture and timescale separation principle involved within the faulty attitude dynamics, a passive FTC scheme was proposed in [13] for a hypersonic vehicle. Similarly, by considering the loss-of-effectiveness actuator faults and uncertainties, and using sliding-mode control (SMC) method, an FTC scheme was designed in [14] for nonlinear systems. In [15], to accommodate the actuator faults, an active FTC scheme was artfully investigated for electric vehicles by integrating a baseline controller, a set of reconfigurable controllers, and a decision mechanism. By simultaneously considering the actuator faults and constraints, an active FTC scheme was developed in [16] to obtain reliable FTC performance. To achieve a safe flight against actuator faults, numerous FTC methods have been designed for UAVs. To utilize the robustness inherent in nonsingular TSMC (NTSMC), a finite-time FTC scheme was designed for a quadrotor UAV by constructing an NTSMC-based inner controller and an NTSMC-based outer controller [17]. By using neural network to learn the fault-induced terms in the backstepping control architecture, a fast FTC method was developed in [18] for UAVs. To counteract the faults and wind disturbances, an FTC was developed in [19] by incorporating fractional-order concept and composite learning algorithm. In [20], high-order sliding-mode differentiator and intelligent learning mechanism were integrated to design the FTC scheme for UAVs. More recently, to increase flight safety, a neural network disturbance observer-based finite-time FTC scheme was developed in [21].

Prescribed performance control (PPC) was initially developed in [22] for constraining tracking errors with predefined error bounds and convergence rates. Recently,

Manuscript received May 02, 2021.
*Corresponding author.
This work was supported by the National Natural Science Foundation of China (62003162, 61833013, 62020106003), the Natural Science Foundation of Jiangsu Province of China (BK20200416), the China Postdoctoral Science Foundation (2020TQ0151; 2020M681590), the State Key Laboratory of Synthetical Automation for Process Industries, Northeastern University (2019-KF-23-05), the 111 Project (B20007), and the Natural Sciences and Engineering Research Council of Canada.

various PPC methods have been reported [23–27]. In [24], a PPC scheme was constructed for pure feedback systems. By combing dynamic surface control and adaptive fuzzy logic, a PPC method was proposed in [26] for constraining the tracking errors. Regarding the PPC of UAV, the authors in [28] proposed a robust PPC scheme for UAVs against payloads. Recently, the PPC concept has been integrated into FTC architecture for further constraining tracking errors when UAV was encountered by actuator faults. In [29], an active FTC strategy was investigated with the integration of fault diagnosis component, such that the prescribed attitude tracking error requirements can be satisfied. Recently, the PPC was further incorporated into the finite-time FTC structure for fixed-wing UAVs to significantly enhance the FTC performance [30]. Although massive FTC methods are effective in handling actuator faults, more effective FTC schemes should be developed towards reliable flights of fixed-wing UAVs.

Motivated by the aforementioned analysis, a proportional-integral-derivative (PID)-type fault-tolerant PPC scheme is proposed for a UAV against actuator faults. First, the tracking errors are converted into a new set of errors using the prescribed performance functions. Then, a PID-type error filter is further adopted to transform the errors. To handle the unknown terms due to actuator faults, a composite learning algorithm with the integration of neural network and disturbance observer is utilized to facilitate the FTC design. Different from existing works, the distinct features of this paper are listed as follows:

(i) In contrast to the FTC methods for UAVs developed in [31–33], which designed the FTC scheme without the consideration of error constraints, PPC is introduced to strictly constrain the tracking errors against actuator faults.

(ii) Different from the composite learning algorithms presented in [20,34], this paper adopts the PID-type error dynamics to design the composite learning algorithm, such that the FTC performance can be significantly enhanced.

(iii) Regarding the massive FTC schemes, which mainly used simulation scenarios to verify the feasibilities of FTC methods, experiments are performed in this paper to show the effectiveness of the FTC scheme.

The remaining structure of this paper is organized as follows. In Section 2, UAV dynamics and fault models are presented. The main result including prescribed performance error transformation, development of composite learning algorithm, and the PID-type FTC design is given in Section 3. Section 4 presents the experimental results. Finally, Section 5 concludes the whole work.

2. Preliminaries and problem statement

2.1 Fixed-wing UAV dynamics

The dynamics of the fixed-wing UAV are as follows [35]:

$$\left\{\begin{aligned} \dot{\mu} &= (p\cos\alpha + r\sin\alpha)/\cos\beta + \dot{\chi}\sin\gamma + \\ &\quad \dot{\chi}\cos\gamma\sin\mu\tan\beta + \dot{\gamma}\cos\mu\tan\beta \\ \dot{\alpha} &= q - \tan\beta(p\cos\alpha + r\sin\alpha) - \\ &\quad (\dot{\chi}\cos\gamma\sin\mu + \dot{\gamma}\cos\mu)/\cos\beta \\ \dot{\beta} &= p\sin\alpha - r\cos\alpha + \dot{\chi}\cos\gamma\cos\mu - \\ &\quad \dot{\gamma}\sin\mu \end{aligned}\right., \tag{1}$$

$$\left\{\begin{aligned} \dot{p} &= (c_1 r + c_2 p)q + c_3\mathcal{L} + c_4\mathcal{N} \\ \dot{q} &= c_5 pr - c_6(p^2 - r^2) + c_7\mathcal{M} \\ \dot{r} &= (c_8 p - c_2 r)q + c_4\mathcal{L} + c_9\mathcal{N} \end{aligned}\right., \tag{2}$$

where μ, α, and β are the bank angle, angle of attack, and sideslip angle, respectively. χ and γ represent the heading angle and flight path angle, respectively. p, q, and r denote the angular rates. $\mathcal{L}$, $\mathcal{M}$, and $\mathcal{N}$ are the roll, pitch, and yaw moments. c_1, c_2, $\cdots$, c_9 represent the inertial terms [36].

$$\left\{\begin{aligned} \dot{\chi} &= (L\sin\mu + Y\cos\mu)/mV\cos\gamma + \\ &\quad T\sin\alpha\sin\mu/mV\cos\gamma - \\ &\quad T\cos\alpha\sin\beta\cos\mu/mV\cos\gamma \\ \dot{\gamma} &= (L\cos\mu - Y\sin\mu)/mV + \\ &\quad T\cos\alpha\sin\beta\sin\mu/mV + \\ &\quad T\sin\alpha\cos\mu/mV - g\cos\gamma/V \end{aligned}\right. \tag{3}$$

where m represents the mass. g is the gravity acceleration. L and Y are the aerodynamic lift and side forces, respectively. V is the velocity, which is updated by the following dynamics:

$$\dot{V} = (-D + T\cos\alpha\cos\beta)/m - g\sin\gamma \tag{4}$$

where T and D denote the thrust and aerodynamic drag forces, respectively.

The aerodynamic forces L, D, Y and the moments $\mathcal{L}$, $\mathcal{M}$, $\mathcal{N}$ can be expressed as

$$\left\{\begin{aligned} & L = \bar{q}sC_L,\ D = \bar{q}sC_D,\ Y = \bar{q}sC_Y \\ & \mathcal{L} = \bar{q}sbC_l,\ \mathcal{M} = \bar{q}scC_m,\ \mathcal{N} = \bar{q}sbC_n \\ & C_L = C_{L0} + C_{L\alpha}\alpha \\ & C_D = C_{D0} + C_{D\alpha}\alpha + C_{D\alpha 2}\alpha^2 \\ & C_Y = C_{Y0} + C_{Y\beta}\beta \\ & C_l = C_{l0} + C_{l\beta}\beta + C_{l\delta_a}\delta_a + C_{l\delta_r}\delta_r + \\ & \qquad C_{lp}bp/2V + C_{lr}br/2V \\ & C_m = C_{m0} + C_{m\alpha}\alpha + C_{m\delta_e}\delta_e + \\ & \qquad C_{mq}cq/2V \\ & C_n = C_{n0} + C_{n\beta}\beta + C_{n\delta_a}\delta_a + C_{n\delta_r}\delta_r + \\ & \qquad C_{np}bp/2V + C_{nr}br/2V \end{aligned}\right. \tag{5}$$

where $\bar{q}=0.5\rho_0 V^2$ is the dynamic pressure with ρ_0 being the air density. s, b, and c are the wing area, wing span, and mean aerodynamic chord, respectively. δ_a, δ_e, and δ_r represent the aileron, elevator, and rudder deflection angles, respectively. The symbols C_{L0}, $C_{L\alpha}$, C_{D0}, $C_{D\alpha}$, $C_{D\alpha 2}$, C_{Y0}, $C_{Y\beta}$, C_{l0}, $C_{l\beta}$, $C_{l\delta_a}$, $C_{l\delta_r}$, C_{lp}, C_{lr}, C_{m0}, $C_{m\alpha}$, $C_{m\delta_e}$, C_{mq}, C_{n0}, $C_{n\beta}$, $C_{n\delta_a}$, $C_{n\delta_r}$, C_{np}, and C_{nr} represent the aerodynamic coefficients.

By defining $\boldsymbol{x}_1=[\mu\ \alpha\ \beta]^{\mathrm{T}}$ and $\boldsymbol{x}_2=[p\ q\ r]^{\mathrm{T}}$, (1) and (2) can be transformed to

$$\dot{\boldsymbol{x}}_1=\boldsymbol{f}_1+\boldsymbol{g}_1\boldsymbol{x}_2, \tag{6}$$

$$\dot{\boldsymbol{x}}_2=\boldsymbol{f}_2+\boldsymbol{g}_2\boldsymbol{u}, \tag{7}$$

where $\boldsymbol{u}=[\delta_a\ \delta_e\ \delta_r]^{\mathrm{T}}$ represents the control input vector. $\boldsymbol{f}_1=[f_{11}\ f_{12}\ f_{13}]^{\mathrm{T}}$, $\boldsymbol{f}_2=[f_{21}\ f_{22}\ f_{23}]^{\mathrm{T}}$, $\boldsymbol{g}_1$ (see (10)), and $\boldsymbol{g}_2=\begin{bmatrix} g_{211} & 0 & g_{213}\\ 0 & g_{222} & 0\\ g_{231} & 0 & g_{233}\end{bmatrix}$ are expressed as

$$\begin{cases} f_{11}=d_1(\sin\gamma+\cos\gamma\sin\mu\tan\beta)+\\ \qquad d_2\cos\mu\tan\beta\\ f_{12}=-d_1\cos\gamma\sin\mu/\cos\beta-\\ \qquad d_2\cos\mu/\cos\beta\\ f_{13}=d_1\cos\gamma\cos\mu-d_2\sin\mu \end{cases}, \tag{8}$$

$$\begin{cases} f_{21}=c_1qr+c_2pq+c_3\bar{q}sb(C_{l0}+C_{l\beta}\beta)+\\ \qquad c_3\bar{q}sb[C_{lp}bp/2V+C_{lr}br/2V]+\\ \qquad c_4\bar{q}sb(C_{n0}+C_{n\beta}\beta)+\\ \qquad c_4\bar{q}sb[C_{np}bp/2V+C_{nr}br/2V]\\ f_{22}=c_5pr-c_6(p^2-r^2)+\\ \qquad c_7\bar{q}sc[C_{m0}+C_{m\alpha}\alpha+C_{mq}cq/2V]\\ f_{23}=c_8pq-c_2qr+c_4\bar{q}sb(C_{l0}+C_{l\beta}\beta)+\\ \qquad c_4\bar{q}sb[C_{lp}bp/2V+C_{lr}br/2V]+\\ \qquad c_9\bar{q}sb(C_{n0}+C_{n\beta}\beta)+\\ \qquad c_9\bar{q}sb[C_{np}bp/2V+C_{nr}br/2V] \end{cases}, \tag{9}$$

$$\boldsymbol{g}_1=\begin{bmatrix} \cos\alpha/\cos\beta & 0 & \sin\alpha/\cos\beta\\ -\cos\alpha\tan\beta & 1 & -\sin\alpha\tan\beta\\ \sin\alpha & 0 & -\cos\alpha \end{bmatrix}, \tag{10}$$

$$\begin{cases} g_{211}=c_3\bar{q}sbC_{l\delta_a}+c_4\bar{q}sbC_{n\delta_a}\\ g_{213}=c_3\bar{q}sbC_{l\delta_r}+c_4\bar{q}sbC_{n\delta_r}\\ g_{222}=c_7\bar{q}scC_{m\delta_e}\\ g_{231}=c_4\bar{q}sbC_{l\delta_a}+c_9\bar{q}sbC_{n\delta_a}\\ g_{233}=c_4\bar{q}sbC_{l\delta_r}+c_9\bar{q}sbC_{n\delta_r} \end{cases}, \tag{11}$$

with d_1 and d_2 being chosen as

$$\begin{cases} d_1=(L\sin\mu+Y\cos\mu)/mV\cos\gamma+\\ \qquad T\sin\alpha\sin\mu/mV\cos\gamma-\\ \qquad T\cos\alpha\sin\beta\cos\mu/mV\cos\gamma\\ d_2=(L\cos\mu-Y\sin\mu)/mV+\\ \qquad T\cos\alpha\sin\beta\sin\mu/mV+\\ \qquad T\sin\alpha\cos\mu/mV-g\cos\gamma/V \end{cases}. \tag{12}$$

2.2 Faulty UAV model against actuator faults

In this paper, the loss-of-effectiveness and bias faults are considered for the aileron, elevator, and rudder actuators of the fixed-wing UAV. The faulty actuator model is expressed by

$$\boldsymbol{u}=\boldsymbol{\rho}\boldsymbol{u}_0+\boldsymbol{b}_f \tag{13}$$

where $\boldsymbol{\rho}=\mathrm{diag}(\rho_1,\rho_2,\rho_3)$ with $0<\rho_1,\rho_2,\rho_3\leqslant 1$ represents the remaining effectiveness matrix. $\boldsymbol{u}$ and $\boldsymbol{u}_0=[\delta_{a0}\ \delta_{e0}\ \delta_{r0}]^{\mathrm{T}}$ represent the applied and commanded input vectors, respectively. $\boldsymbol{b}_f=[b_{f1}\ b_{f2}\ b_{f3}]^{\mathrm{T}}$ is the bounded bias fault vector.

By substituting (13) into (7), one can obtain the following faulty UAV model:

$$\dot{\boldsymbol{x}}_1=\boldsymbol{f}_1+\boldsymbol{g}_1\boldsymbol{x}_2, \tag{14}$$

$$\dot{\boldsymbol{x}}_2=\boldsymbol{f}_2+\boldsymbol{g}_2\boldsymbol{\rho}\boldsymbol{u}_0+\boldsymbol{g}_2\boldsymbol{b}_f. \tag{15}$$

2.3 Control objective

The control objective is to design the control input $\boldsymbol{u}_0$ for the faulty UAV models (14) and (15), such that the attitude vector $\boldsymbol{x}_1$ can track the desired attitude vector against actuator faults, and the tracking errors are strictly constrained within the prescribed error bounds.

3. Main results

In this section, prescribed performance functions and a PID-type error filter are first used to transform the errors. Moreover, to counteract the faults, a composite learning algorithm with the neural network and the disturbance observer is artfully proposed for enhancing flight safety.

3.1 Prescribed performance-based error transformation

Define the desired attitude vector as $\boldsymbol{x}_{1d}=[\mu_d\ \alpha_d\ \beta_d]$ and the attitude tracking error as $\tilde{\boldsymbol{x}}_1=[\tilde{x}_{11}\ \tilde{x}_{12}\ \tilde{x}_{13}]^{\mathrm{T}}=\boldsymbol{x}_1-\boldsymbol{x}_{1d}$, then one has

$$\dot{\tilde{\boldsymbol{x}}}_1=\dot{\boldsymbol{x}}_1-\dot{\boldsymbol{x}}_{1d}=\boldsymbol{f}_1+\boldsymbol{g}_1\boldsymbol{x}_2-\dot{\boldsymbol{x}}_{1d}. \tag{16}$$

One can further obtain

$$\begin{aligned}\ddot{\tilde{\boldsymbol{x}}}_1 = {}& \dot{\boldsymbol{f}}_1 + \dot{\boldsymbol{g}}_1\boldsymbol{x}_2 + \boldsymbol{g}_1\boldsymbol{f}_2 + \\ & \boldsymbol{g}_1\boldsymbol{g}_2\boldsymbol{\rho}\boldsymbol{u}_0 + \boldsymbol{g}_1\boldsymbol{g}_2\boldsymbol{b}_f - \ddot{\boldsymbol{x}}_{1d}\,. \end{aligned} \tag{17}$$

To constrain the attitude tracking error $\tilde{\boldsymbol{x}}_{1d}$, the following error constraints are first introduced:

$$-\underline{k}_i\varepsilon_i(t) \leqslant \tilde{x}_{1i} \leqslant \overline{k}_i\varepsilon_i(t) \tag{18}$$

where $i = 1,2,3$, $\underline{k}_i > 0$ and $\overline{k}_i > 0$ are design parameters. $-\underline{k}_i\varepsilon_i(t)$ and $\overline{k}_i\varepsilon_i(t)$ are the prescribed lower and upper bounds, respectively. $\varepsilon_i(t)$ is the prescribed performance function, given by

$$\varepsilon_i(t) = (\varepsilon_{i0} - \varepsilon_{i\infty})\mathrm{e}^{-\eta_i t} + \varepsilon_{i\infty} \tag{19}$$

where ε_{i0} and $\varepsilon_{i\infty}$ represent the initial and final values of the prescribed performance function. η_i denotes the allowable convergence rate.

By using the prescribed performance function (19), the prescribed error bounds at the initial time and the steady-state phase can be described as $\left[-\underline{k}_i\varepsilon_{i0},\ \overline{k}_i\varepsilon_{i0}\right]$ and $\left[-\underline{k}_i\varepsilon_{i\infty},\ \overline{k}_i\varepsilon_{i\infty}\right]$, respectively. The parameters $\underline{k}_i$ and $\overline{k}_i$ are set to satisfy $\tilde{x}_i(0) \in \left[-\underline{k}_i\varepsilon_{i0},\ \overline{k}_i\varepsilon_{i0}\right]$, where $\tilde{x}_i(0)$ is the initial value, $i = 1,2,3$.

To design the PPC scheme, the error constraint inequality (18) is changed to the following equality:

$$\tilde{x}_{1i} = \varepsilon_i\varLambda_i(s_{1i}) \tag{20}$$

where $i = 1,2,3$, s_{1i} is the transformed error. $\varLambda_i(\cdot)$ is the transformation function with the following properties:

(i) $\varLambda_i(0) = 0$,

(ii) $-\underline{k}_i \leqslant \varLambda_i(s_{1i}) \leqslant \overline{k}_i$,

(iii) $\lim\limits_{s_{1i}\to\infty} \varLambda_i(s_{1i}) = \overline{k}_i$,

(iv) $\lim\limits_{s_{1i}\to-\infty} \varLambda_i(s_{1i}) = -\underline{k}_i$.

In this paper, $\varLambda_i(\cdot)$ is chosen as

$$\varLambda_i(s_{1i}) = \frac{\overline{k}_i\mathrm{e}^{s_{1i}+\sigma_i} - \underline{k}_i\mathrm{e}^{-s_{1i}-\sigma_i}}{\mathrm{e}^{s_{1i}+\sigma_i} + \mathrm{e}^{-s_{1i}-\sigma_i}} \tag{21}$$

where $\sigma_i = \dfrac{1}{2}\ln\dfrac{\underline{k}_i}{\overline{k}_i}$.

Then, one has

$$s_{1i} = \varLambda^{-1}\left(\frac{\tilde{x}_{1i}}{\varepsilon_i}\right) = \frac{1}{2}\ln\frac{\overline{k}_i\underline{k}_i + \overline{k}_i\nu_i}{\overline{k}_i\underline{k}_i - \underline{k}_i\nu_i} \tag{22}$$

where $\nu_i = \dfrac{\tilde{x}_{1i}}{\varepsilon_i}$.

Taking the time derivative of (22) yields

$$\begin{aligned}\dot{s}_{1i} = {}& \frac{1}{2}\frac{\overline{k}_i\underline{k}_i - \underline{k}_i\nu_i}{\overline{k}_i\underline{k}_i + \overline{k}_i\nu_i}\left[\frac{\mathrm{d}}{\mathrm{d}t}\left(\frac{\overline{k}_i\underline{k}_i + \overline{k}_i\nu_i}{\overline{k}_i\underline{k}_i - \underline{k}_i\nu_i}\right)\right] = \\ & \frac{1}{2\varepsilon_i}\left(\frac{1}{\underline{k}_i + \sigma_i} - \frac{1}{\underline{k}_i - \sigma_i}\right)\cdot\left(\dot{\tilde{x}}_{1i} - \frac{\tilde{x}_{1i}\dot{\varepsilon}_i}{\varepsilon_i}\right) = \\ & \xi_i\left(\dot{\tilde{x}}_{1i} - \frac{\tilde{x}_{1i}\dot{\varepsilon}_i}{\varepsilon_i}\right)\end{aligned} \tag{23}$$

where $\xi_i = \dfrac{1}{2\varepsilon_i}\left(\dfrac{1}{\underline{k}_i + \sigma_i} - \dfrac{1}{\underline{k}_i - \sigma_i}\right)$.

By writing (23) into the compact form, one has

$$\dot{\boldsymbol{s}}_1 = \boldsymbol{\xi}\left(\dot{\tilde{\boldsymbol{x}}}_1 - \boldsymbol{\varepsilon}^{-1}\dot{\boldsymbol{\varepsilon}}\tilde{\boldsymbol{x}}_1\right) \tag{24}$$

where $\boldsymbol{s}_1 = [s_{11}\ s_{12}\ s_{13}]^{\mathrm{T}}$, $\boldsymbol{\xi} = \mathrm{diag}(\xi_1,\xi_2,\xi_3)$, and $\boldsymbol{\varepsilon} = \mathrm{diag}(\varepsilon_1,\varepsilon_2,\varepsilon_3)$.

3.2 Composite learning-based PID fault-tolerant prescribed performance control (PIDFTPPC) design and stability analysis

In this subsection, the prescribed performance error (22) is first transformed by using the PID-type filter, and then a composite learning algorithm is developed to handle the fault-induced nonlinear terms within the PID-type error dynamics by integrating the neural network and the disturbance observer.

Taking the time derivative of (24) gives

$$\begin{aligned}\ddot{\boldsymbol{s}}_1 = {}& \dot{\boldsymbol{\xi}}\dot{\tilde{\boldsymbol{x}}}_1 - \dot{\boldsymbol{\xi}}\boldsymbol{\varepsilon}^{-1}\dot{\boldsymbol{\varepsilon}}\tilde{\boldsymbol{x}}_1 + \boldsymbol{\xi}\boldsymbol{\varepsilon}^{-1}\dot{\boldsymbol{\varepsilon}}\boldsymbol{\varepsilon}^{-1}\dot{\boldsymbol{\varepsilon}}\tilde{\boldsymbol{x}}_1 + \\ & \boldsymbol{\xi}\ddot{\tilde{\boldsymbol{x}}}_1 - \boldsymbol{\xi}\boldsymbol{\varepsilon}^{-1}\ddot{\boldsymbol{\varepsilon}}\tilde{\boldsymbol{x}}_1 - \boldsymbol{\xi}\boldsymbol{\varepsilon}^{-1}\dot{\boldsymbol{\varepsilon}}\dot{\tilde{\boldsymbol{x}}}_1\,.\end{aligned} \tag{25}$$

Introduce the following PID-type error filter:

$$\boldsymbol{e} = 2k_1k_2\boldsymbol{s}_1 + k_1^2k_2\int_0^t \boldsymbol{s}_1\mathrm{d}\tau + k_2\dot{\boldsymbol{s}}_1 \tag{26}$$

where k_1 and k_2 are positive constants, such that the transfer function $s^2 + 2k_1s + k_1^2$ is Hurwitz.

By considering (24), (25), and (26), one has

$$\begin{aligned}\dot{\boldsymbol{e}} = {}& 2k_1k_2\dot{\boldsymbol{s}}_1 + k_1^2k_2\boldsymbol{s}_1 + k_2\dot{\boldsymbol{\xi}}\dot{\tilde{\boldsymbol{x}}}_1 - k_2\dot{\boldsymbol{\xi}}\boldsymbol{\varepsilon}^{-1}\dot{\boldsymbol{\varepsilon}}\tilde{\boldsymbol{x}}_1 + \\ & k_2\boldsymbol{\xi}\boldsymbol{\varepsilon}^{-1}\dot{\boldsymbol{\varepsilon}}\boldsymbol{\varepsilon}^{-1}\dot{\boldsymbol{\varepsilon}}\tilde{\boldsymbol{x}}_1 + k_2\boldsymbol{\xi}\ddot{\tilde{\boldsymbol{x}}}_1 - k_2\boldsymbol{\xi}\boldsymbol{\varepsilon}^{-1}\ddot{\boldsymbol{\varepsilon}}\tilde{\boldsymbol{x}}_1 - \\ & k_2\boldsymbol{\xi}\boldsymbol{\varepsilon}^{-1}\dot{\boldsymbol{\varepsilon}}\dot{\tilde{\boldsymbol{x}}}_1\end{aligned} \tag{27}$$

By substituting (17) into (27), one has

$$\begin{aligned}\dot{\boldsymbol{e}} = {}& 2k_1k_2\dot{\boldsymbol{s}}_1 + k_1^2k_2\boldsymbol{s}_1 + k_2\dot{\boldsymbol{\xi}}\dot{\tilde{\boldsymbol{x}}}_1 - k_2\dot{\boldsymbol{\xi}}\boldsymbol{\varepsilon}^{-1}\dot{\boldsymbol{\varepsilon}}\tilde{\boldsymbol{x}}_1 + \\ & k_2\boldsymbol{\xi}\boldsymbol{\varepsilon}^{-1}\dot{\boldsymbol{\varepsilon}}\boldsymbol{\varepsilon}^{-1}\dot{\boldsymbol{\varepsilon}}\tilde{\boldsymbol{x}}_1 + k_2\boldsymbol{\xi}\dot{\boldsymbol{f}}_1 + k_2\boldsymbol{\xi}\dot{\boldsymbol{g}}_1\boldsymbol{x}_2 + \\ & k_2\boldsymbol{\xi}\boldsymbol{g}_1\boldsymbol{f}_2 + k_2\boldsymbol{\xi}\boldsymbol{g}_1\boldsymbol{g}_2\boldsymbol{\rho}\boldsymbol{u}_0 - k_2\boldsymbol{\xi}\ddot{\boldsymbol{x}}_{1d} - \\ & k_2\boldsymbol{\xi}\boldsymbol{\varepsilon}^{-1}\ddot{\boldsymbol{\varepsilon}}\tilde{\boldsymbol{x}}_1 - k_2\boldsymbol{\xi}\boldsymbol{\varepsilon}^{-1}\dot{\boldsymbol{\varepsilon}}\dot{\tilde{\boldsymbol{x}}}_1 = \\ & 2k_1k_2\dot{\boldsymbol{s}}_1 + k_1^2k_2\boldsymbol{s}_1 + k_2\boldsymbol{\xi}\boldsymbol{g}_1\boldsymbol{g}_2\boldsymbol{u}_0 - \\ & k_2\boldsymbol{\xi}\ddot{\boldsymbol{x}}_{1d} + \boldsymbol{F}\end{aligned} \tag{28}$$

where the strongly nonlinear function $\boldsymbol{F}$ is expressed as

$$\begin{aligned}\boldsymbol{F} = {}& k_2\dot{\boldsymbol{\xi}}\dot{\tilde{\boldsymbol{x}}}_1 - k_2\dot{\boldsymbol{\xi}}\boldsymbol{\varepsilon}^{-1}\dot{\boldsymbol{\varepsilon}}\tilde{\boldsymbol{x}}_1 + k_2\boldsymbol{\xi}\boldsymbol{\varepsilon}^{-1}\dot{\boldsymbol{\varepsilon}}\boldsymbol{\varepsilon}^{-1}\dot{\boldsymbol{\varepsilon}}\tilde{\boldsymbol{x}}_1 + \\ & k_2\boldsymbol{\xi}\dot{\boldsymbol{f}}_1 + k_2\boldsymbol{\xi}\dot{\boldsymbol{g}}_1\boldsymbol{x}_2 + k_2\boldsymbol{\xi}\boldsymbol{g}_1\boldsymbol{f}_2 + \\ & k_2\boldsymbol{\xi}\boldsymbol{g}_1\boldsymbol{g}_2\boldsymbol{\rho}\boldsymbol{u}_0 - k_2\boldsymbol{\xi}\boldsymbol{g}_1\boldsymbol{g}_2\boldsymbol{u}_0 - \\ & k_2\boldsymbol{\xi}\boldsymbol{\varepsilon}^{-1}\ddot{\boldsymbol{\varepsilon}}\tilde{\boldsymbol{x}}_1 - k_2\boldsymbol{\xi}\boldsymbol{\varepsilon}^{-1}\dot{\boldsymbol{\varepsilon}}\dot{\tilde{\boldsymbol{x}}}_1\,.\end{aligned} \tag{29}$$

In this paper, the composite learning algorithm presented in [34] is used to approximate the strongly nonlinear function $\boldsymbol{F}$ by integrating neural network and disturbance observer. From (29), it can be seen that $\boldsymbol{u}_0$ is involved in $\boldsymbol{F}$, which causes the algebraic loops. To address this, the Butterworth low-pass filter technique is further used to break the algebraic loop by filtering the signal $\boldsymbol{u}_0$ within (29) before sending it to the composite learning algorithm, such that $\boldsymbol{F}=\boldsymbol{F}_\varrho+\boldsymbol{e}_f$, where $\boldsymbol{F}_\varrho$ is the radial basis function neural network (RBFNN), $\boldsymbol{e}_f$ is the bounded filter error [37].

Introduce the error prediction $\boldsymbol{\varUpsilon}=\boldsymbol{e}-\hat{\boldsymbol{e}}$, where $\hat{\boldsymbol{e}}$ is updated by the following expression:

$$\begin{aligned}\dot{\hat{\boldsymbol{e}}} =&\hat{\boldsymbol{W}}^{*\mathrm{T}}\boldsymbol{\varphi}+\hat{\boldsymbol{D}}+2k_1k_2\dot{\boldsymbol{s}}_1+k_1^2k_2\boldsymbol{s}_1+\\ &k_2\boldsymbol{\xi}\boldsymbol{g}_1\boldsymbol{g}_2\boldsymbol{u}_0-k_2\boldsymbol{\xi}\ddot{\boldsymbol{x}}_{1d}+k_3\boldsymbol{\varUpsilon}\end{aligned}\tag{30}$$

where $\boldsymbol{F}_\varrho=\boldsymbol{W}^{*\mathrm{T}}\boldsymbol{\varphi}+\boldsymbol{\epsilon}$ is used in (30), $\boldsymbol{W}^*$ and $\boldsymbol{\varphi}$ represent the optimal weighting matrix and the Gaussian function vector, respectively. $k_3>0$ is a positive parameter. $\boldsymbol{\epsilon}$ represents the bounded approximation error vector. $\boldsymbol{D}=\boldsymbol{e}_f+\boldsymbol{\epsilon}$ is the lumped error. $\hat{\boldsymbol{W}}^*$ and $\hat{\boldsymbol{D}}$ represent the estimations of $\boldsymbol{W}^*$ and $\boldsymbol{D}$, respectively.

Based on the prediction error $\boldsymbol{\varUpsilon}=\boldsymbol{e}-\hat{\boldsymbol{e}}$, the following disturbance observer is developed to estimate $\boldsymbol{D}$:

$$\begin{cases}\hat{\boldsymbol{D}}=\boldsymbol{\eta}+k_4\boldsymbol{e}\\ \dot{\boldsymbol{\eta}}=-k_4\boldsymbol{\eta}-k_4\left[\hat{\boldsymbol{W}}^{*\mathrm{T}}\boldsymbol{\varphi}+2k_1k_2\dot{\boldsymbol{s}}_1+k_1^2k_2\boldsymbol{s}_1+\right.\\ \quad k_2\boldsymbol{\xi}\boldsymbol{g}_1\boldsymbol{g}_2\boldsymbol{u}_0-k_2\boldsymbol{\xi}\ddot{\boldsymbol{x}}_{1d}+\\ \quad \left. k_4\boldsymbol{e}-k_4^{-1}(k_5\boldsymbol{\varUpsilon}+\boldsymbol{e})\right]\end{cases}\tag{31}$$

where $k_4>0$ is a positive parameter.

To estimate $\boldsymbol{W}^*$, the following adaptive law is designed:

$$\dot{\hat{\boldsymbol{W}}}^*=k_6\left[\boldsymbol{\varphi}(k_5\boldsymbol{\varUpsilon}+\boldsymbol{e})^{\mathrm{T}}-k_7\hat{\boldsymbol{W}}^*\right]\tag{32}$$

where $k_5>0$, $k_6>0$, and $k_7>0$ are positive parameters.

Design the control signal $\boldsymbol{u}_0$ as

$$\begin{aligned}\boldsymbol{u}_0 =&(k_2\boldsymbol{\xi}\boldsymbol{g}_1\boldsymbol{g}_2)^{-1}\left(-\boldsymbol{k}_8\boldsymbol{e}-2k_1k_2\dot{\boldsymbol{s}}_1-k_1^2k_2\boldsymbol{s}_1\right)+\\ &(k_2\boldsymbol{\xi}\boldsymbol{g}_1\boldsymbol{g}_2)^{-1}\left(k_2\boldsymbol{\xi}\ddot{\boldsymbol{x}}_{1d}-\hat{\boldsymbol{W}}^{*\mathrm{T}}\boldsymbol{\varphi}-\hat{\boldsymbol{D}}\right)\end{aligned}\tag{33}$$

where $\boldsymbol{k}_8$ is a positive diagonal matrix.

The time derivative of $\boldsymbol{\varUpsilon}=\boldsymbol{e}-\hat{\boldsymbol{e}}$ is

$$\begin{aligned}\dot{\boldsymbol{\varUpsilon}}=\dot{\boldsymbol{e}}-&\left[\hat{\boldsymbol{W}}^{*\mathrm{T}}\boldsymbol{\varphi}+\hat{\boldsymbol{D}}+2k_1k_2\dot{\boldsymbol{s}}_1+k_1^2k_2\boldsymbol{s}_1+\right.\\ &\left.k_2\boldsymbol{\xi}\boldsymbol{g}_1\boldsymbol{g}_2\boldsymbol{u}_0-k_2\boldsymbol{\xi}\ddot{\boldsymbol{x}}_{1d}+k_3\boldsymbol{\varUpsilon}\right]=\\ &\tilde{\boldsymbol{W}}^{*\mathrm{T}}\boldsymbol{\varphi}+\tilde{\boldsymbol{D}}-k_3\boldsymbol{\varUpsilon}.\end{aligned}\tag{34}$$

Similarly, one has

$$\begin{aligned}\dot{\hat{\boldsymbol{D}}}=&-k_4\boldsymbol{\eta}-k_4\left[\hat{\boldsymbol{W}}^{*\mathrm{T}}\boldsymbol{\varphi}+2k_1k_2\dot{\boldsymbol{s}}_1+\right.\\ &k_1^2k_2\boldsymbol{s}_1+k_2\boldsymbol{\xi}\boldsymbol{g}_1\boldsymbol{g}_2\boldsymbol{u}_0-k_2\boldsymbol{\xi}\ddot{\boldsymbol{x}}_{1d}+\\ &\left.k_4\boldsymbol{e}-k_4^{-1}(k_5\boldsymbol{\varUpsilon}+\boldsymbol{e})\right]+k_4\dot{\boldsymbol{e}}=\\ &k_4\tilde{\boldsymbol{D}}+k_4\tilde{\boldsymbol{W}}^{*\mathrm{T}}\boldsymbol{\varphi}+k_5\boldsymbol{\varUpsilon}+\boldsymbol{e}\end{aligned}\tag{35}$$

where $\tilde{\boldsymbol{W}}^*=\boldsymbol{W}^*-\hat{\boldsymbol{W}}^*$ and $\tilde{\boldsymbol{D}}=\boldsymbol{D}-\hat{\boldsymbol{D}}$ are the estimation errors of the optimal weighting matrix and the disturbance observer, respectively.

To this end, the proposed FTC scheme can be summarized as Fig. 1.

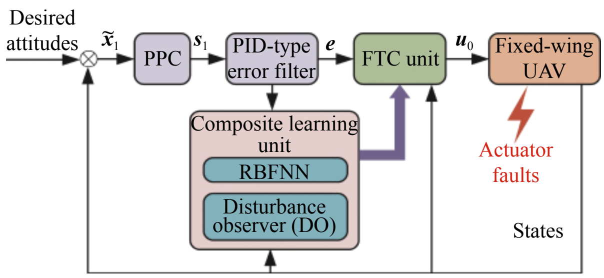

Fig. 1 Structure of the developed FTC scheme

Theorem 1 Consider the UAV systems (1) and (2) against actuator faults, if the FTC scheme is developed by the prescribed performance error transformation (22), the PID-type error filter (26), the disturbance observer (31), the neural adaptive law (32), and the control signal (33), then the attitude vector of the fixed-wing UAV can reach to the desired attitudes. Moreover, the attitude tracking errors $\tilde{\boldsymbol{x}}_1=[\tilde{x}_{11}\ \tilde{x}_{12}\ \tilde{x}_{13}]^{\mathrm{T}}$ and errors $\tilde{\boldsymbol{W}}^*$, $\tilde{\boldsymbol{D}}$, $\boldsymbol{\varUpsilon}$ are uniformly ultimately bounded (UUB). The attitude tracking errors $\tilde{\boldsymbol{x}}_1=[\tilde{x}_{11}\ \tilde{x}_{12}\ \tilde{x}_{13}]^{\mathrm{T}}$ are strictly confined within the prescribed error bounds.

Proof Choose the following Lyapunov function candidate:

$$\begin{aligned}L=&\frac{1}{2}\boldsymbol{e}^{\mathrm{T}}\boldsymbol{e}+\frac{1}{2}k_5\boldsymbol{\varUpsilon}^{\mathrm{T}}\boldsymbol{\varUpsilon}+\\ &\frac{1}{2}\tilde{\boldsymbol{D}}^{\mathrm{T}}\tilde{\boldsymbol{D}}+\frac{1}{2k_6}\mathrm{tr}\left(\tilde{\boldsymbol{W}}^{*\mathrm{T}}\tilde{\boldsymbol{W}}^*\right).\end{aligned}\tag{36}$$

Differentiating (36) with (28) yields

$$\begin{aligned}\dot{L}=&\boldsymbol{e}^{\mathrm{T}}\left(-\boldsymbol{k}_8\boldsymbol{e}+\tilde{\boldsymbol{W}}^{*\mathrm{T}}\boldsymbol{\varphi}+\tilde{\boldsymbol{D}}\right)+\\ &\tilde{\boldsymbol{D}}^{\mathrm{T}}\left(\dot{\boldsymbol{D}}-k_4\tilde{\boldsymbol{D}}-k_4\tilde{\boldsymbol{W}}^{*\mathrm{T}}\boldsymbol{\varphi}-k_5\boldsymbol{\varUpsilon}-\boldsymbol{e}\right)-\\ &\mathrm{tr}\left[\tilde{\boldsymbol{W}}^{*\mathrm{T}}\boldsymbol{\varphi}(k_5\boldsymbol{\varUpsilon}+\boldsymbol{e})^{\mathrm{T}}-k_7\tilde{\boldsymbol{W}}^{*\mathrm{T}}\hat{\boldsymbol{W}}^*\right]+\\ &k_5\boldsymbol{\varUpsilon}^{\mathrm{T}}\tilde{\boldsymbol{W}}^{*\mathrm{T}}\boldsymbol{\varphi}+k_5\boldsymbol{\varUpsilon}^{\mathrm{T}}\tilde{\boldsymbol{D}}-k_3k_5\boldsymbol{\varUpsilon}^{\mathrm{T}}\boldsymbol{\varUpsilon}.\end{aligned}\tag{37}$$

By using the following inequalities:

$$\begin{cases}\mathrm{tr}\left(\tilde{\boldsymbol{W}}^{*\mathrm{T}}\boldsymbol{W}^*\right)\leqslant\dfrac{\mathrm{tr}\left(\tilde{\boldsymbol{W}}^{*\mathrm{T}}\tilde{\boldsymbol{W}}^*\right)}{2}+\dfrac{\mathrm{tr}\left(\boldsymbol{W}^{*\mathrm{T}}\boldsymbol{W}^*\right)}{2}\\ \tilde{\boldsymbol{D}}^{\mathrm{T}}\dot{\boldsymbol{D}}\leqslant\dfrac{\tilde{\boldsymbol{D}}^{\mathrm{T}}\tilde{\boldsymbol{D}}}{2}+\dfrac{1}{2}D_m\\ -\tilde{\boldsymbol{D}}^{\mathrm{T}}\tilde{\boldsymbol{W}}^{\mathrm{T}}\boldsymbol{\varphi}\leqslant\dfrac{\tilde{\boldsymbol{D}}^{\mathrm{T}}\tilde{\boldsymbol{D}}}{2}+\dfrac{\bar{\varphi}\mathrm{tr}\left(\tilde{\boldsymbol{W}}^{*\mathrm{T}}\tilde{\boldsymbol{W}}^*\right)}{2}\end{cases},\tag{38}$$

one has

$$\begin{aligned}
\dot{L} = &\, \boldsymbol{e}^{\mathrm{T}}\left(-\boldsymbol{k}_8\boldsymbol{e}+\tilde{\boldsymbol{W}}^{*\mathrm{T}}\boldsymbol{\varphi}+\tilde{\boldsymbol{D}}\right)+\\
&\tilde{\boldsymbol{D}}^{\mathrm{T}}\left(\dot{\boldsymbol{D}}-k_4\tilde{\boldsymbol{D}}-k_4\tilde{\boldsymbol{W}}^{*\mathrm{T}}\boldsymbol{\varphi}-k_5\boldsymbol{\varUpsilon}-\boldsymbol{e}\right)-\\
&\mathrm{tr}\left[\tilde{\boldsymbol{W}}^{*\mathrm{T}}\boldsymbol{\varphi}(k_5\boldsymbol{\varUpsilon}+\boldsymbol{e})^{\mathrm{T}}-k_7\tilde{\boldsymbol{W}}^{*\mathrm{T}}\hat{\boldsymbol{W}}^{*}\right]-\\
&(k_5\boldsymbol{\varUpsilon}+\boldsymbol{e})^{\mathrm{T}}\tilde{\boldsymbol{W}}^{*\mathrm{T}}\boldsymbol{\varphi}+k_7\mathrm{tr}\left(\tilde{\boldsymbol{W}}^{*\mathrm{T}}\boldsymbol{W}^{*}\right)-\\
&k_7\mathrm{tr}\left(\tilde{\boldsymbol{W}}^{*\mathrm{T}}\tilde{\boldsymbol{W}}^{*}\right)+k_5\boldsymbol{\varUpsilon}^{\mathrm{T}}\tilde{\boldsymbol{W}}^{*\mathrm{T}}\boldsymbol{\varphi}+k_5\boldsymbol{\varUpsilon}^{\mathrm{T}}\tilde{\boldsymbol{D}}-k_3k_5\boldsymbol{\varUpsilon}^{\mathrm{T}}\boldsymbol{\varUpsilon}\leqslant\\
&\boldsymbol{e}^{\mathrm{T}}\left(-\boldsymbol{k}_8\boldsymbol{e}+\tilde{\boldsymbol{W}}^{*\mathrm{T}}\boldsymbol{\varphi}+\tilde{\boldsymbol{D}}\right)+\\
&\tilde{\boldsymbol{D}}^{\mathrm{T}}\left(\dot{\boldsymbol{D}}-k_4\tilde{\boldsymbol{D}}-k_4\tilde{\boldsymbol{W}}^{*\mathrm{T}}\boldsymbol{\varphi}-k_5\boldsymbol{\varUpsilon}-\boldsymbol{e}\right)-\\
&\mathrm{tr}\left[\tilde{\boldsymbol{W}}^{*\mathrm{T}}\boldsymbol{\varphi}(k_5\boldsymbol{\varUpsilon}+\boldsymbol{e})^{\mathrm{T}}-k_7\tilde{\boldsymbol{W}}^{*\mathrm{T}}\hat{\boldsymbol{W}}^{*}\right]-\\
&(k_5\boldsymbol{\varUpsilon}+\boldsymbol{e})^{\mathrm{T}}\tilde{\boldsymbol{W}}^{*\mathrm{T}}\boldsymbol{\varphi}+\frac{k_7}{2}\mathrm{tr}\left(\tilde{\boldsymbol{W}}^{*\mathrm{T}}\tilde{\boldsymbol{W}}^{*}\right)+\\
&\frac{k_7}{2}\mathrm{tr}\left(\boldsymbol{W}^{*\mathrm{T}}\boldsymbol{W}^{*}\right)-k_7\mathrm{tr}\left(\tilde{\boldsymbol{W}}^{*\mathrm{T}}\tilde{\boldsymbol{W}}^{*}\right)+\\
&k_5\boldsymbol{\varUpsilon}^{\mathrm{T}}\tilde{\boldsymbol{W}}^{*\mathrm{T}}\boldsymbol{\varphi}+k_5\boldsymbol{\varUpsilon}^{\mathrm{T}}\tilde{\boldsymbol{D}}-k_3k_5\boldsymbol{\varUpsilon}^{\mathrm{T}}\boldsymbol{\varUpsilon}\leqslant\\
&\boldsymbol{e}^{\mathrm{T}}\left(-\boldsymbol{k}_8\boldsymbol{e}+\tilde{\boldsymbol{W}}^{*\mathrm{T}}\boldsymbol{\varphi}+\tilde{\boldsymbol{D}}\right)+\\
&\tilde{\boldsymbol{D}}^{\mathrm{T}}\left(\dot{\boldsymbol{D}}-k_4\tilde{\boldsymbol{D}}-k_4\tilde{\boldsymbol{W}}^{*\mathrm{T}}\boldsymbol{\varphi}-k_5\boldsymbol{\varUpsilon}-\boldsymbol{e}\right)-\\
&\mathrm{tr}\left[\tilde{\boldsymbol{W}}^{*\mathrm{T}}\boldsymbol{\varphi}(k_5\boldsymbol{\varUpsilon}+\boldsymbol{e})^{\mathrm{T}}-k_7\tilde{\boldsymbol{W}}^{*\mathrm{T}}\hat{\boldsymbol{W}}^{*}\right]-\\
&(k_5\boldsymbol{\varUpsilon}+\boldsymbol{e})^{\mathrm{T}}\tilde{\boldsymbol{W}}^{*\mathrm{T}}\boldsymbol{\varphi}-\frac{k_7}{2}\mathrm{tr}\left(\tilde{\boldsymbol{W}}^{*\mathrm{T}}\tilde{\boldsymbol{W}}^{*}\right)+\\
&\frac{k_7}{2}\mathrm{tr}\left(\boldsymbol{W}^{*\mathrm{T}}\boldsymbol{W}^{*}\right)+k_5\boldsymbol{\varUpsilon}^{\mathrm{T}}\tilde{\boldsymbol{W}}^{*\mathrm{T}}\boldsymbol{\varphi}+\\
&k_5\boldsymbol{\varUpsilon}^{\mathrm{T}}\tilde{\boldsymbol{D}}-k_3k_5\boldsymbol{\varUpsilon}^{\mathrm{T}}\boldsymbol{\varUpsilon}. \qquad (39)
\end{aligned}$$

Equation (39) can be further transformed to the following expression:

$$\begin{aligned}
\dot{L}\leqslant &-\boldsymbol{e}^{\mathrm{T}}\boldsymbol{k}_8\boldsymbol{e}+\tilde{\boldsymbol{D}}^{\mathrm{T}}\dot{\boldsymbol{D}}-k_4\tilde{\boldsymbol{D}}^{\mathrm{T}}\tilde{\boldsymbol{D}}-\\
&k_4\tilde{\boldsymbol{D}}^{\mathrm{T}}\tilde{\boldsymbol{W}}^{*\mathrm{T}}\boldsymbol{\varphi}-\frac{k_7}{2}\mathrm{tr}\left(\tilde{\boldsymbol{W}}^{*\mathrm{T}}\tilde{\boldsymbol{W}}^{*}\right)+\\
&\frac{k_7}{2}\mathrm{tr}\left(\boldsymbol{W}^{*\mathrm{T}}\boldsymbol{W}^{*}\right)-k_3k_5\boldsymbol{\varUpsilon}^{\mathrm{T}}\boldsymbol{\varUpsilon}\leqslant\\
&-\boldsymbol{e}^{\mathrm{T}}\boldsymbol{k}_8\boldsymbol{e}-\left(\frac{k_4}{2}-\frac{1}{2}\right)\tilde{\boldsymbol{D}}^{\mathrm{T}}\tilde{\boldsymbol{D}}-\\
&\left(\frac{k_7}{2}-\frac{k_4\bar{\varphi}}{2}\right)\mathrm{tr}\left(\tilde{\boldsymbol{W}}^{*\mathrm{T}}\tilde{\boldsymbol{W}}^{*}\right)-\\
&k_3k_5\boldsymbol{\varUpsilon}^{\mathrm{T}}\boldsymbol{\varUpsilon}+\frac{\bar{D}}{2}+\frac{k_7}{2}\mathrm{tr}\left(\boldsymbol{W}^{*\mathrm{T}}\boldsymbol{W}^{*}\right)\leqslant\\
&-\zeta_1L+\zeta_2 \qquad (40)
\end{aligned}$$

where ζ_1 and ζ_2 are respectively expressed as

$$\zeta_1=\min\left\{\ 2\lambda_{\min}(\boldsymbol{k}_8),k_4-1,(k_7-k_4\bar{\varphi})k_6,2k_3\ \right\}>0, \quad (41)$$

$$\zeta_2=\frac{\bar{D}}{2}+\frac{k_7}{2}\mathrm{tr}\left(\boldsymbol{W}^{*\mathrm{T}}\boldsymbol{W}^{*}\right). \quad (42)$$

By using Lyapunov theorem, $\tilde{\boldsymbol{x}}_1=[\tilde{x}_{11}\ \tilde{x}_{12}\ \tilde{x}_{13}]^{\mathrm{T}}$, $\tilde{\boldsymbol{W}}^{*}$, $\tilde{\boldsymbol{D}}$, and $\boldsymbol{\varUpsilon}$ are UUB. Moreover, the error $\boldsymbol{s}_1$ is UUB once the uniformly ultimate boundedness of $\boldsymbol{e}$ is achieved. Then, considering the relationship between the attitude tracking error $\tilde{\boldsymbol{x}}_1$ and the prescribed performance error $\boldsymbol{s}_1$, one can obtain that $\tilde{\boldsymbol{x}}_1$ is convergent and strictly controlled within the prescribed error ranges $\left[-\underline{k}_i\varepsilon_i(t),\ \overline{k}_i\varepsilon_i(t)\right]$. □

Remark 1 In the previous work [34], a composite adaptive FTC scheme was proposed for UAVs with prescribed error requirements. The disturbance observer and neural network are designed to learn the fault-induced nonlinear terms within the prescribed performance error dynamics. In this paper, a PID-type error filter is further introduced for improving the FTC performance, and then the composite learning algorithm presented in [34] is modified to learn the fault-induced unknown terms within the PID-type error dynamics.

4. HIL experimental results

In this section, hardware-in-the-loop (HIL) experiments are performed for showing the effectiveness of the proposed PIDFTPPC scheme. The structural parameters and aerodynamic coefficients of the fixed-wing UAV can be referred to [35]. The developed HIL testbed is shown in Fig. 2, which has been used to verify the feasibility of the control scheme presented in [21] and consists of an open-source Pixhawk 4 autopilot hardware with the STM32F765 processor and a mobile workstation Thinkpad P52. In the HIL experiment, the Pixhawk 4 autopilot hardware and the P52 workstation are used to run the FTC algorithm and the fixed-wing UAV dynamics, respectively.

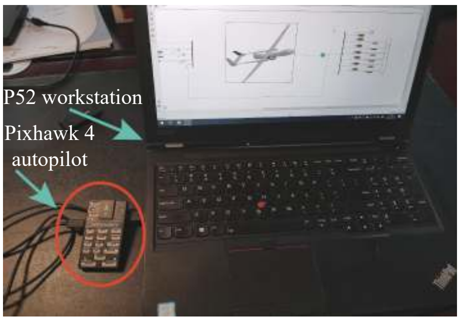

Fig. 2 HIL testbed

The design parameters are chosen as $k_1=20$, $k_2=11.6$, $k_3=2$, $k_4=1.5$, $k_5=3.2$, $k_6=10$, $k_7=0.4$, $\boldsymbol{k}_8=\mathrm{diag}(20,20,20)$, $\eta_1=0.2$, $\eta_2=0.2$, $\eta_3=0.2$, $\overline{k_1}=0.6$, $\underline{k_1}=0.6$, $\overline{k_2}=0.6$, $\underline{k_2}=0.6$, $\overline{k_3}=0.6$, $\underline{k_3}=0.6$, $\varepsilon_{10}=1.72$, $\varepsilon_{1\infty}=0.57$, $\varepsilon_{20}=4.58$, $\varepsilon_{2\infty}=2.29$, $\varepsilon_{30}=1.72$, and $\varepsilon_{3\infty}=0.29$. To show the superiority of the proposed PIDFTPPC scheme, the comparative backstepping control (BSC) scheme is adopted by removing the prescribed performance functions, PID-type error filter, and composite learning algorithm.

Fig. 3 illustrates the response curves of the bank angle, angle of attack, and sideslip angle of the fixed-wing UAV under the PIDFTPPC and BSC schemes. By using the PIDFTPPC strategy, the states can reach to the desired attitude references even under the initial tracking errors and the fixed-wing UAV is encountered by the aileron, elevator, and rudder faults at t = 15 s, 30 s, 45 s sequentially. From Fig. 3(b), it is observed that large angle of attack deviations are caused by employing the BSC scheme.

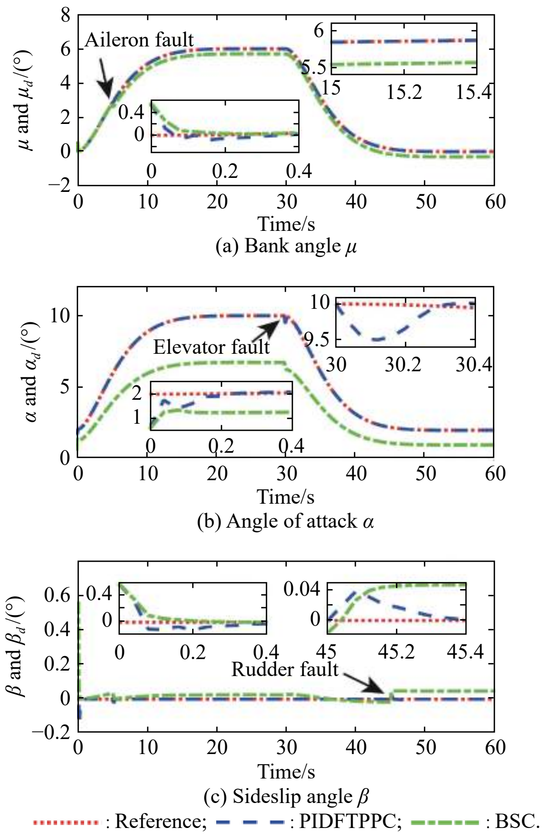

Fig. 3 Reseponse curves

Fig. 4 presents the attitude tracking errors $\tilde{x}_{11}=\mu-\mu_d$, $\tilde{x}_{12}=\alpha-\alpha_d$, and $\tilde{x}_{13}=\beta-\beta_d$ under the PIDFTPPC and BSC schemes. At the beginning of the HIL experiment, the initial bank angle, angle of attack, and sideslip angle tracking errors are 0.57°, −1.43°, and 0.57°, respectively. Then, with the developed PIDFTPPC scheme, these initial tracking errors are pulled into the very small region containing zero. When the aileron, elevator, and rudder actuators of the fixed-wing UAV are abruptly injected by the faults at t = 15 s, 30 s, 45 s, respectively, slightly degraded performance is induced. Then, the composite learning unit is activated to compensate for the faults, such that the errors are reduced and flight safety can be enhanced. Moreover, with the help of the incorporated prescribed performance functions, the attitude errors $\tilde{x}_{11}$, $\tilde{x}_{12}$, and $\tilde{x}_{13}$ are strictly confined within the prescribed bounds $\left[-\underline{k}_1\varepsilon_1(t),\overline{k}_1\varepsilon_1(t)\right]$, $\left[-\underline{k}_2\varepsilon_2(t),\overline{k}_2\varepsilon_2(t)\right]$, $\left[-\underline{k}_3\varepsilon_3(t),\overline{k}_3\varepsilon_3(t)\right]$, respectively. However, large tracking errors occur when the comparative BSC scheme is used to steer the fixed-wing UAV to track its desired references. It can be seen from Fig. 4(b) that the angle of attack tracking errors are outside of the prescribed lower bound.

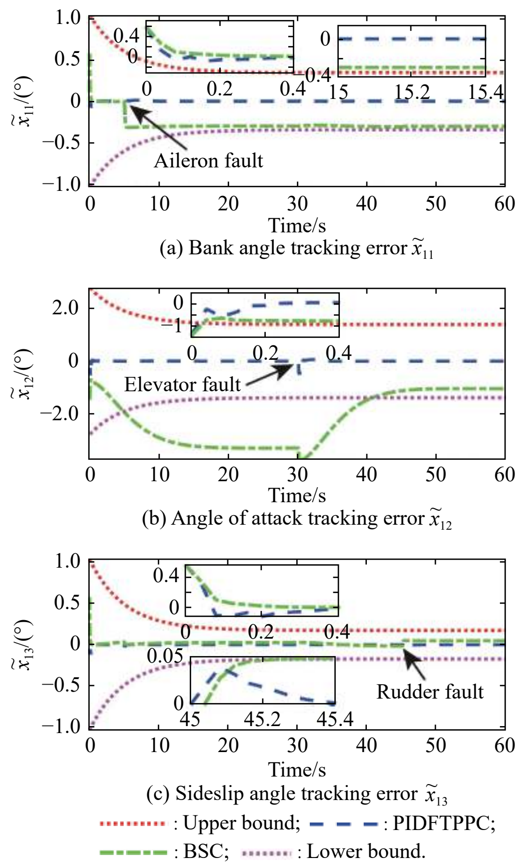

Fig. 4 Attitude tracking erros

Fig. 5 presents the aileron, elevator, and rudder deflection angles under the PIDFTPPC and BSC schemes. By using the PIDFTPPC scheme, the control inputs, i.e., the aileron, elevator, and rudder deflection angles, adjust the signals to attenuate the adverse effects caused by the faults at t = 15 s, 30 s, 45 s. It can be observed that the comparative BSC scheme has a weak adjustment capability to react to the actuator faults, leading to weaken FTC performance, which can be seen from the Fig. 3 and Fig. 4.

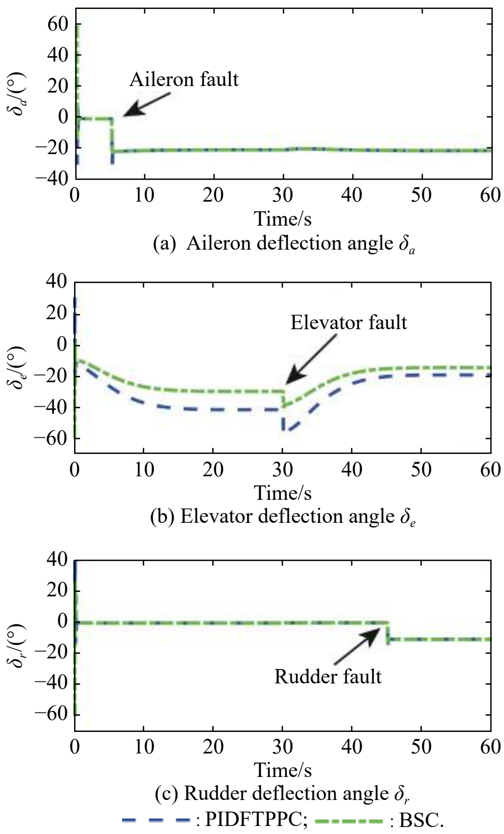

Fig. 5 Aileron, elevator and rudder deflection angles

5. Conclusions

In this paper, a PIDFTPPC scheme has been developed for a fixed-wing UAV. The prescribed performance functions and PID-type filter are integrated to convert the attitude tracking errors and then a composite learning algorithm with neural network and disturbance observer has been developed to compensate for the fault-induced nonlinear terms. Lyapunov stability analysis has shown that the tracking errors are uniformly ultimately bounded and thoroughly confined within the specified ranges. Comparative HIL experiments have been conducted to show the superiority of the proposed control scheme.

References

[1] LIU P, CHEN A Y, HUANG Y, et al. A review of rotorcraft unmanned aerial vehicle (UAV) developments and applications in civil engineering. Smart Structures and Systems, 2014, 13(6): 1065–1094.

[2] ZHANG C, KOVACS J M. The application of small unmanned aerial systems for precision agriculture: a review. Precision Agriculture, 2012, 13(6): 693–712.

[3] SAEED A S, YOUNES A B, CAI C, et al. A survey of hybrid unmanned aerial vehicles. Progress in Aerospace Sciences, 2018, 98: 91–105.

[4] HU X X, MA H W, YE Q S, et al. Hierarchical method of task assignment for multiple cooperating UAV teams. Journal of Systems Engineering and Electronics, 2015, 26(5): 1000–1009.

[5] ZHANG Y M, JIANG J. Bibliographical review on reconfigurable fault-tolerant control systems. Annual Reviews in Control, 2008, 32(2): 229–252.

[6] JIANG B, ZHANG K, LIU C, et al. Fault diagnosis and accommodation with flight control applications. Journal of Control and Decision, 2020, 7(1): 24–43.

[7] CONG L, QIN H L, TAN Z Z. Intelligent fault-tolerant algorithm with two-stage and feedback for integrated navigation federated filtering. Journal of Systems Engineering and Electronics, 2011, 22(2): 274–282.

[8] XU Y F, JIANG B, GAO Z F, et al. Fault tolerant control for near space vehicle: a survey and some new results. Journal of Systems Engineering and Electronics, 2011, 22(1): 88–94.

[9] REN Z, WANG W, SHEN Z. New robust fault-tolerant controller for self-repairing flight control systems. Journal of Systems Engineering and Electronics, 2011, 22(1): 77–82.

[10] YU Z Q, ZHANG Y M, JIANG B, et al. A review on fault-tolerant cooperative control of multiple unmanned aerial vehicles. Chinese Journal of Aeronautics, 2021. DOI: 10.1016/j.cja.2021.04.022.

[11] ZHOU D H, ZHAO Y H, WANG Z D, et al. Review on diagnosis techniques for intermittent faults in dynamic systems. IEEE Trans. on Industrial Electronics, 2019, 67(3): 2337–2347.

[12] MENG L, JIANG B. Backstepping-based active fault-tolerant control for a class of uncertain SISO nonlinear systems. Journal of Systems Engineering and Electronics, 2009, 20(6): 1263–1270.

[13] CAO T, GAO Z F, QIAN M S, et al. Passive fault tolerant control approach for hypersonic vehicle with actuator loss of effectiveness faults. Proc. of the Chinese Control and Decision Conference, 2016: 5951−5956.

[14] NASIRI A, NGUANG S K, SWAIN A, et al. Passive actuator fault tolerant control for a class of MIMO nonlinear systems with uncertainties. International Journal of Control, 2019, 92(3): 693–704.

[15] ZHANG G G, ZHANG H, HUANG X Y, et al. Active fault-tolerant control for electric vehicles with independently driven rear in-wheel motors against certain actuator faults. IEEE Trans. on Control Systems Technology, 2015, 24(5): 1557–1572.

[16] SHEN Q, YUE C F, GOH C H, et al. Active fault-tolerant control system design for spacecraft attitude maneuvers with actuator saturation and faults. IEEE Trans. on Industrial Electronics, 2018, 66(5): 3763–3772.

[17] HOU Z W, LU P, TU Z J. Nonsingular terminal sliding mode control for a quadrotor UAV with a total rotor failure. Aerospace Science and Technology, 2020, 98: 105716.

[18] YU Z Q, LIU Z X, ZHANG Y M, et al. Distributed finite-time fault-tolerant containment control for multiple unmanned aerial vehicles. IEEE Trans. on Neural Networks and Learning Systems, 2019, 31(6): 2077–2091.

[19] YU Z Q, ZHANG Y M, JIANG B, et al. Composite adaptive disturbance observer-based decentralized fractional-order fault-tolerant control of networked UAVs. IEEE Trans. on Systems, Man, and Cybernetics: Systems, 2020. DOI: 10.1109/TSMC.2020.3010678.

[20] YU Z Q, ZHANG Y M, JIANG B, et al. Decentralized fractional-order backstepping fault-tolerant control of multi-UAVs against actuator faults and wind effects. Aerospace Science and Technology, 2020, 104: 105939.

[21] YU Z Q, ZHANG Y M, JIANG B, et al. Nussbaum-based finite-time fractional-order backstepping fault-tolerant flight control of fixed-wing UAV against input saturation with hardware-in-the-loop validation. Mechanical Systems and Signal Processing, 2021, 153: 107406.

[22] BECHLIOULIS C P, ROVITHAKIS G A. Robust adaptive

control of feedback linearizable MIMO nonlinear systems with prescribed performance. IEEE Trans. on Automatic Control, 2008, 53(9): 2090–2099.

[23] LI Y M, TONG S C. Adaptive neural networks prescribed performance control design for switched interconnected uncertain nonlinear systems. IEEE Trans. on Neural Networks and Learning Systems, 2017, 29(7): 3059–3068.

[24] BECHLIOULIS C P, ROVITHAKIS G A. Approximation-free prescribed performance control for unknown SISO pure feedback systems. Proc. of the European Control Conference, 2013: 1557−1572.

[25] ZHAO K, SONG Y D, MA T D, et al. Prescribed performance control of uncertain Euler-Lagrange systems subject to full-state constraints. IEEE Trans. on Neural Networks and Learning Systems, 2018, 29(8): 3478–3489.

[26] HAN S I, LEE J M. Partial tracking error constrained fuzzy dynamic surface control for a strict feedback nonlinear dynamic system. IEEE Trans. on Fuzzy Systems, 2013, 22(5): 1049–1061.

[27] THEODORAKOPOULOS A, ROVITHAKIS G A. Low-complexity prescribed performance control of uncertain MIMO feedback linearizable systems. IEEE Trans. on Automatic Control, 2015, 61(7): 1946–1952.

[28] HUA C C, CHEN J, GUAN X P. Adaptive prescribed performance control of QUAVs with unknown time-varying payload and wind gust disturbance. Journal of the Franklin Institute, 2018, 355(14): 6323–6338.

[29] QIAN M, JIANG B, LIU H H. Dynamic surface active fault tolerant control design for the attitude control systems of UAV with actuator fault. International Journal of Control, Automation and Systems, 2016, 14(3): 723–732.

[30] YU Z Q, ZHANG Y M, LIU Z X, et al. Decentralized finite-time adaptive fault-tolerant synchronization tracking control for multiple UAVs with prescribed performance. Journal of the Franklin Institute, 2020, 357(16): 11830−11862.

[31] YU Z Q, ZHANG Y M, JIANG B, et al. Distributed adaptive fault-tolerant close formation flight control of multiple trailing fixed-wing UAVs. ISA Transactions, 2020, 106: 181–199.

[32] YU Z Q, QU Y H, ZHANG Y M. Distributed fault-tolerant cooperative control for multi-UAVs under actuator fault and input saturation. IEEE Trans. on Control Systems Technology, 2018, 27(6): 2417–2429.

[33] CHOWDHARY G, JOHNSON E N, CHANDRAMOHAN R, et al. Guidance and control of airplanes under actuator failures and severe structural damage. Journal of Guidance, Control, and Dynamics, 2013, 36(4): 1093–1104.

[34] YU Z Q, LIU Z X, ZHANG Y M, et al. Decentralized fault-tolerant cooperative control of multiple UAVs with prescribed attitude synchronization tracking performance under directed communication topology. Frontiers of Information Technology & Electronic Engineering, 2019, 20(5): 685–700.

[35] YU Z Q, ZHANG Y M, LIU Z X, et al. Distributed adaptive fractional-order fault-tolerant cooperative control of networked unmanned aerial vehicles via fuzzy neural networks. IET Control Theory & Applications, 2019, 13(17): 2917–2929.

[36] YU Z Q, QU Y H, ZHANG Y M. Safe control of trailing UAV in close formation flight against actuator fault and wake vortex effect. Aerospace Science and Technology, 2018, 77: 189–205.

[37] ZOU A, HOU Z, TAN M. Adaptive control of a class of nonlinear pure-feedback systems using fuzzy backstepping approach. IEEE Trans. on Fuzzy Systems, 2008, 16(4): 886–897.

Biographies

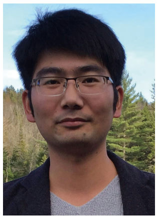

YU Ziquan received his Ph.D. degree in control science and engineering from Northwestern Polytechnical University, Xi'an, China, in 2019. From 2017 to 2019, he was a joint Ph.D. student supported by the China Scholarship Council with the Department of Mechanical, Industrial and Aerospace Engineering, Concordia University, Montreal, QC, Canada. He is currently with the College of Automation Engineering, Nanjing University of Aeronautics and Astronautics, Nanjing, China. His current research interests include fault-tolerant cooperative control of safety-critical systems, and guidance, navigation, and control of unmanned aerial vehicles.

E-mail: yuziquan@nuaa.edu.cn

ZHANG Youmin received his B.S., M.S., and Ph.D. degrees in automatic control from Northwestern Polytechnical University, Xi 'an, China, in 1983, 1986, and 1995, respectively. He is currently a professor with the Department of Mechanical, Industrial and Aerospace Engineering and the Concordia Institute of Aerospace Design and Innovation, Concordia University, Montreal, QC, Canada. He has authored seven books, more than 550 journal and conference papers, and book chapters. His current research interests include guidance, navigation, and control (GNC), fault detection and diagnosis (FDD), fault-tolerant control (FTC), and remote sensing with applications to unmanned aerial/space/ground/ marine vehicles, smart grids, and smart cities. Dr. Zhang is a fellow of CSME, a senior member of AIAA and IEEE, and a member of Technical Committee for several scientific societies. He is an editorial board member, deputy editor-in-chief, editor/associate editor of several international journals, including Journal of Intelligent & Robotic Systems, IEEE Trans. on Neural Networks and Learning Systems, and Guidance, Navigation and Control. He has served as the general chair, program chair, and IPC Member of several unmanned systems and renewable energies relevant international conferences, including as general chair and honorary general chair of the 2020, 2021, and 2022 International Conference on Unmanned Aircraft Systems (ICUAS), respectively.

E-mail: ymzhang@encs.concordia.ca

JIANG Bin received his Ph.D. degree in automatic control from Northeastern University, Shenyang, China, in 1995. He has been a postdoctoral fellow or a research fellow in Singapore, France, and the USA, and a visiting professor in Canada. He is currently a chair professor of Cheung Kong Scholar Program in Ministry of Education, and vice president in Nanjing University of Aeronautics and Astronautics, Nanjing, China. His current research interests include fault diagnosis and fault-tolerant control and their applications. Dr. Jiang serves as an editor, an associate editor or an editorial board member for the IEEE Trans. on Cybernetics, IEEE Trans. on Neural Networks and Learning Systems, International Journal of Control, Automation Systems, Neurocomputing, Acta Automatica Sinica, and Journal of Astronautics. He is IEEE fellow and the chair of the Control Systems Chapter of the IEEE Nanjing Section and a member of the International Federation of Automatic Control Technical Committee on Fault Detection, Supervision, and Safety of Technical Processes.

E-mail: binjiang@nuaa.edu.cn